Aggregation and Porin-like Channel Activity of a β Sheet Peptide

Jyothi Thundimadathil, Roger W. Roeske, Hao-Yuan Jiang, and Lili Guo*

Department of Biochemistry and Molecular Biology, Indiana University School of Medicine, Indianapolis, Indiana 46202

Received May 10, 2005; Revised Manuscript Received June 7, 2005

ABSTRACT: β sheet peptides (e.g., amyloid β) are known to form ion channels in lipid bilayers possibly through aggregation, though the channel structure is not clear. We have recently reported that a short β sheet peptide, $(xSxG)_6$, forms porin-like voltage-gated channels in lipid bilayers [Thundimadathil et al. (2005) *Biochem. Biophys. Res. Commun. 330,* 585−590]. To account for the porin-like activity, oligomerization of the peptide into a β barrel-like structure was proposed. In this work, peptide aggregation in aqueous and membrane environments and a detailed study of channel properties were performed to gain insight into the mechanism of channel formation. The complex nature of the channel was revealed by kinetic analysis and the occurrence of interconverting multiple conductance states. Ion channels were inhibited by Congo red, suggesting that the peptide aggregates are the active channel species. Peptide aggregation and fibril formation in water were confirmed by electron microscopy (EM) and Congo red binding studies. Furthermore, oligomeric structures in association with lipid bilayers were detected. Circular dichroism of peptide-incorporated liposomes and peptide−lipid binding studies using EM suggest a lipid-induced β sheet aggregation. Gel electrophoresis of peptide-incorporated liposomes showed dimeric and multimeric structures. Taken together, this work indicates insertion of $(xSxG)_6$ as oligomers into the lipid bilayer, followed by rearrangement into a β barrel-like pore structure. A large peptide pore comprising several individual β sheets or smaller β sheet aggregates is expected to have a complex behavior in membranes. A dyad repeat sequence and the presence of glycine, serine, and hydrophobic residues in a repeated pattern in this peptide may be providing a favorable condition for the formation of a β barrel-like structure in lipid bilayers.

The aggregation of β sheet proteins and the formation of amyloid fibril deposits are characteristic features of a variety of human pathologies such as Alzheimer's disease, prion disorders, and type 2 diabetes (*1*−*4*). It has been proposed that the cytotoxic action of amyloid β proteins might be initiated by the interaction with cell membranes and subsequent formation of ion channels (*5*, *6*). The ion channels were inhibited by Congo red, a dye used as a diagnostic test for amyloid structures, suggesting that the channels were formed by peptide aggregation in membranes (*7*). Moreover, binding studies of β sheet peptides in lipid membranes indicate a lipid-induced β sheet aggregation and further emphasize the role of lipid membranes in β sheet aggregation (*8*, *9*). Hence it is argued that the structural properties of peptides that form β sheet and aggregate into fibrils suit them for membrane insertion and channel formation (*10*). Another unrelated example is provided by a 24-residue synthetic peptide analogue of a leucine-rich repeat motif, which was shown to have significant β sheet content in membranes compared to that in solution and formed ion channels in lipid bilayers (*11*).

Though several aggregating β sheet peptides are found to form multimeric ion channels in membranes, the structure responsible for their ion channel activity is not clear. Atomic force microscopy (AFM)[1] imaging studies of Aβ peptides revealed the formation of doughnut-shaped structures protruding out of the membrane surface with a centralized pore-like depression presumably representing individual channels (*12*). Theoretical models of Aβ peptides suggest a transmembrane annular polymeric structure (*6*). The formation of β barrel structures similar to the pore structures described for porins was also speculated (*7*). Porins are pore-forming proteins found in the outer membrane of Gram-negative bacteria, mitochondria, and chloroplast (*13*−*16*). These proteins form one of the two distinct structural classes of integral membrane proteins called β barrel membrane proteins (transmembrane β barrels, TMBs) as they have membrane-spanning segments formed by antiparallel β strands creating a channel in the form of a β barrel. In addition to these native proteins, the β barrel motif is also used by a large diverse set of secreted membrane-permeabilizing protein toxins (pore-forming toxins or PFTs) that assemble into β barrels on exogenous membranes (*17*, *18*).

* To whom correspondence should be addressed. Phone: (317) 274-7507. Fax: (317) 274-4686. E-mail: lguo@iupui.edu.

[1] Abbreviations: AFM, atomic force microscopy; HBTU, 2-(1*H*-benzotriazol-1-yl)-1,1,3,3-tetramethyluronium hexafluorophosphate; HOBT, 1-hydroxybenzotriazole; DIEA, *N*,*N*-diisopropylethylamine; NMP, *N*-methylpyrrolidone; TFA, trifluoroacetic acid; DPhPC, diphytanoylphosphatidylcholine; DMPC, dimyristoylphosphatidylcholine; DCM, dichloromethane; TFE, trifluoroethanol; RP-HPLC, reverse-phase high-performance liquid chromatography; MALDI-TOF, matrix-assisted laser desorption ionization time of flight; FTIR, Fourier transform infrared spectroscopy; ATR, attenuated total reflection; CD, circular dichroism; MRW, mean residual ellipticity; EM, electron microscopy; SDS−PAGE, sodium dodecyl sulfate−polyacrylamide gel electrophoresis; PFT, pore-forming toxins; Aβ, amyloid β; TMB, transmembrane β barrel.

10.1021/bi0508643 CCC: $30.25
Published on Web 07/09/2005

The main difference between TMBs and PFTs is that, in the former, a β barrel is formed by the folding of a single polypeptide chain while, in the latter, it is formed through the association of several individual β strand monomers. In general, the formation of high-conductance, voltage-gated (two-state gating of individual channels with closing at both positive and negative applied potentials) channels exhibiting several subconductance states and a complex kinetic behavior is a characteristic feature of β barrel porins (*19*−*21*). It is believed that the two-state voltage-dependent gating is a fundamental feature of β barrel proteins. Though the aggregation and self-assembly of the above-mentioned Aβ peptides into a β barrel structure are possible in principle, there has been no evidence of a close similarity between their ion channel characteristics and that of β barrel porins (*22*).

Recently, we observed the formation of porin-like high-conductance voltage-gated channels by a short synthetic β sheet peptide [VSLGLSIGFSVGVSIGWSFGRSRG, abbreviated as $(xSxG)_6$] in lipid bilayer membranes (*23*). Ion channel formation by this β sheet peptide is not surprising as several other β sheet peptides also form channels as explained before (*5*−*7*, *10*). However, the formation of porin-like channels indicates organization of β sheets into an ordered molecular architecture in membranes.

In this paper we tried to address a basic question, why does $(xSxG)_6$ show conformational and electrophysiological similarities to that of β barrel porins? A detailed analysis of the ion channel characteristics of the peptide has been performed to gain insight into the complex nature of the channel. A short peptide as a monomer is not expected to form a β barrel structure in membranes, and hence special emphasis has been given to peptide aggregation studies in the aqueous and membrane environment using electron microscopy (EM), Congo red binding, and gel electrophoresis to understand the mechanism of channel formation. The effect of Congo red on the channel activity is also evaluated. Formation of ion channels was inhibited by Congo red, suggesting that the peptide aggregates are the active channel species. The observation of oligomeric structures in association with lipid vesicles indicates insertion of peptide as large oligomers into lipid bilayers. Circular dichroism and EM of peptide−liposome samples suggest a lipid-induced β sheet aggregation. On the basis of the aggregation studies and ion channel characteristics, the formation of a complex β barrel-like pore comprising several individual β sheets or smaller β sheet aggregates is suggested. The presence of glycine, serine, and hydrophobic residues in a repeated pattern into a dyad repeat sequence may be providing a favorable condition for the formation of a β barrel-like structure in lipid bilayers.

MATERIALS AND METHODS

Materials. Reagents for peptide synthesis, viz., 2-(1*H*-benzotriazol-1-yl)-1,1,3,3-tetramethyluronium hexafluorophosphate (HBTU), 1-hydroxybenzotriazole (HOBT), *N*,*N*-diisopropylethylamine (DIEA), *N*-methylpyrrolidone (NMP), dichloromethane, piperidine, trifluoroacetic acid (TFA), and Kaiser reagent, were of peptide synthesis grade purchased from Applied Biosystems (Foster City, CA). Gly-wang resin and Fmoc-protected amino acids were available from Advanced Chem Tech (Louisville, KY). All other solvents used were of HPLC grade purchased from Fisher Scientific (Fair Lawn, NJ). Diphytanoylphosphatidylcholine (DPhPC) and dimyristoylphosphatidylcholine (DMPC) were purchased from Avanti Polar Lipids (Alabaster, AL). Sodium dodecyl sulfate (SDS), acrylamide monomer (electrophoresis grade), methylenebis(acrylamide) (electrophoresis grade), ammonium persulfate (APS; electrophoresis grade), and *N*,*N*,*N*′,*N*′-tetramethylethylenediamine (TEMED; electrophoresis grade) were obtained from Bio-Rad (Hercules, CA). Tris−tricine was purchased from Sigma (St. Louis, MO).

Peptide Synthesis, Purification, and Characterization. The $(xSxG)_6$ peptide was synthesized using a standard solid-phase Fmoc chemistry starting with Gly-wang resin (0.1 mmol scale) and HBTU/HOBT in NMP as a coupling agent. After the synthesis, the peptide was cleaved from the resin using a cleavage mixture containing TFA (10 mL), phenol (0.5 g), H_2O (0.5 mL), triisopropylsilane (0.25 mL), 1, 2-ethanedithiol (0.25 mL), and thioanisole (0.5 mL) under nitrogen. After the cleavage and deprotection, the solvent was evaporated and the peptide was precipitated using ether. The precipitated peptide was washed with ether and lyophilized. It was purified by reverse-phase HPLC (Varian Prostar 210 system fitted with a Prostar 320 UV/vis detector) on a C_4 column (Vydac; 5 μm particle size; 10 mm i.d. and 250 mm length). A methanol−water gradient [solution A, 100% H_2O and 0.1% TFA; solution B, 100% CH_3OH and 0.09% TFA; program, B 70% (0 min)−70% (20 min)−90% (39 min)−90% (60 min)−95% (61 min)−100% (85 min)] was used and the peptide eluted after 62 min. The collected methanol−water fractions were lyophilized after removing methanol by rotary evaporation. The peptide was soluble in TFE and DMSO (>5 and 10 mg/mL, respectively), and solubility in other solvents decreased with decrease in polarity of the solvents. The solubility in different alcohols decreased in the order methanol > ethanol > 2-propanol > octanol. The molecular weight of the peptide was confirmed using a MALDI-TOF mass spectrometer (Micromass, Manchester, U.K.). The observed mass (2426.20) was close to the calculated value (2426.11). The purity of the peptide was >95%.

Prediction of Transmembrane β Strands. A web-based program, PRED-TMBB (http://bioinformatics.biol.uoa.gr/PRED-TMBB) based on a hidden Markov model capable of predicting the transmembrane β strands of the Gram-negative bacteria outer membrane proteins and discriminating such proteins from water-soluble ones, has been used to check for any similarity between the peptide sequence in the study and that of transmembrane barrels (*24*). Upon submitting the peptide sequence, the server reported a score indicating the probability of the peptide being an outer membrane β barrel protein, posterior probabilities for the transmembrane strand prediction, and a graphical representation of the assumed position of the transmembrane strands with respect to the lipid bilayer. Proteins producing a score lower than a predefined threshold are considered to be β barrel membrane proteins. Two neural network methods, B2TMPRED and TM-BETA, were also used for comparison (*25*, *26*).

Peptide−Unilamellar Lipid Vesicles. Small unilamellar vesicles were prepared by a modified method of Wallace and Blout (*27*). About 0.5 mg of peptide and 5 mg of DMPC

(peptide:lipid molar ratio 1:36) were codissolved in 2 mL of trifluoroethanol followed by the subsequent removal of the solvent to get a peptide−lipid film. The lipid film was hydrated with 500 μL of D_2O and incubated at 40 °C for 2 h followed by sonication for 5−10 min using a Branson sonifier 450 (output control 4, duty cycle 30%, 35 W) fitted with a contact tip accessory. Samples were centrifuged at 14000 rpm for 10 min at room temperature to remove any suspended particulates. After these treatments a clear solution was obtained. Liposome without peptide was also prepared as a control.

IR Spectroscopy. ATR-FTIR spectra were recorded on a Perkin-Elmer 2000 spectrometer. Typically, aliquots of 50 μL of peptide-incorporated liposome samples were loaded onto a ZnSe internal reflection element (IRE), and a hydrated thin film was formed by using a stream of nitrogen gas. The IRE was then placed in an ATR accessory, and FTIR spectra were collected. The background spectrum was collected using the same IRE before the sample measurements. Fourier deconvoluted and second derivative spectra were obtained using Grams analyst 2000 software. The resulting spectra were smoothed by a 7-point Savitsky−Golay function. Band fitting of the deconvoluted spectra was done using a Gaussian function, and starting band parameters were taken from deconvoluted spectra. The initial line widths were set to 12 cm^{-1} and allowed to vary freely. The relative areas of the components were expressed as a percentage of the area of each fitted region, which was equivalent to an area normalization of the amide bands.

Circular Dichroism Spectroscopy. CD measurements were carried out at 20 °C on a JASCO J-720 spectrometer. The ellipticity was calibrated with (+)-10-camphorsulfonic acid. Each spectrum was an average of 6−30 scans using quartz cells having path lengths of 0.01 or 0.05 cm. Spectra were recorded in the range 260−180 nm at a speed of 50 nm/min with a resolution of 0.2 nm and are presented on a per amide basis (deg cm^2 $dmol^{-1}$). The spectra were corrected by subtracting the blank spectra of corresponding solvents and liposomes used for the study. The mean residue molar ellipticity $[\Theta]_{MRW}$ was calculated using the formula $[\Theta]_{MRW} = \Theta/(10C_r l)$, where C_r is the mean residue molar concentration ($C_r = nC_p$, where n is the number of peptide bonds and C_p is the molar concentration in moles per liter), l is the path length in centimeters, and Θ is the ellipticity in millidegrees. For secondary structure determination of the peptide the ellipticity is expressed as $\Delta\epsilon_{MRW}$ in M^{-1} cm^{-1} units ($\Delta\epsilon_{MRW} = [\Theta]_{MRW}/3298$). To estimate the secondary structure content of the peptide, an analysis of the relevant CD spectra was carried out using the CDPro software available from the web site http://lamar.colostate.edu/~sreeram/CDPro, developed by Sreerama and Woody (*28*−*31*). An extended protein basis set of 43 soluble and 13 membrane proteins (basis set 10) was used for analysis. The analysis was performed using three methods, CDSSTR, CONTIN/LL, and SELCON3. In general, CONTIN/LL, a self-consistent method with an incorporated variable selection procedure, produced the most reliable results (*30*). In some cases we also estimated the percentage α helix from $\Delta\epsilon$ at 222 nm and the percentage of β strand from overall CD magnitude as previously described (Zhong and Johnson) for comparison (*32*).

Planar Lipid Bilayer Studies. Planar lipid bilayers were formed across a 200 μm diameter aperture in the wall of a Delrin cup (*33*). Lipid bilayer forming solution contained DPhPC at a concentration of 15 mg/mL in *n*-decane. Membranes used in the experiment were stable and had conductance of less than 10 pS up to voltages of ±150 mV prior to the addition of peptide. About 3 μL of a methanolic solution of the peptide (0.05 mg/mL) was added to one side of the bilayer chamber, defined as cis, containing 100−1000 mM CsCl solution (unbuffered) to a final concentration of $\sim 10^{-8}$ M. The other side of the bilayer was defined as trans and was the virtual ground. The Ag/AgCl electrodes were connected to the cis and trans chambers through 1 M KCl−agar bridges. A custom current/voltage conversion amplifier was used to optimize single channel recording. The data were digitized at 2 kHz and filtered at 1 kHz using a 16-bit data acquisition system (Digidata 1320 A; Axon Instruments, Union City, CA) and an 8-pole Bessel filter (Warner Instrument Corp., Hamden, CT). Data were acquired and analyzed using pClamp software (Axon Instruments). Curve fits were done using the Marquardt least-squares algorithm.

Electron Microscopy. Electron micrographs of peptide fibrils and liposomes were acquired by using a Tecnai G2 12 Bio Twin electron microscope (FEI, Hillsboro, OR) operated at 80 kV. Digitized images were taken with an AMT (Advanced Microscopy Techniques Corp., Danvers, MA) XR60-2K CCD camera. To make fibrils, 100 μL of a methanolic solution of $(xSxG)_6$ peptide (2 mg/mL) diluted to 1000 μL with water was incubated at 60 °C for about 2 h and aged overnight. A 5 μL aliquot of the sample was placed on a carbon/Formvar-coated 200 mesh copper grid and allowed to absorb for 1 min. The sample was then negatively stained with a drop of 1% alcoholic uranyl acetate solution for 30 s. After wicking off the excess stain, the grid was allowed to air-dry and viewed at magnifications of 25000−200000.

Congo Red Binding. Congo red binding experiments were performed as described elsewhere (*34*). Ten microliters of a suspension of peptide fibril was added to 240 μL of 25 μM Congo red in 100 mM sodium phosphate buffer with 150 mM NaCl, pH 7.4. After a 30 min incubation period, an ultraviolet absorbance spectrum was recorded. A red shift of 20−30 nm in the absorbance maximum of Congo red (486 nm) and hyperchromaticity are indicative of Congo red binding.

Gel Electrophoresis. The aggregation state of the peptide in a lipid environment was assessed by observing the migration patterns following sodium dodecyl sulfate (SDS)−polyacrylamide gel electrophoresis (PAGE). The peptide-incorporated liposome sample (peptide:lipid ratio 1:36) was prepared by sonication as explained before. After peptide−liposome samples were suspended in loading buffer (10 mM Tris-HCl, 1 mM EDTA, 3% SDS, 20 mM dithiothreitol, 10% glycerol, 0.1% bromphenol blue), the SDS−PAGE was carried out at 100 V using 16.5% acrylamide gel in the presence of Tris−tricine buffer, and the gels were stained with 0.1% Coomassie Brilliant Blue (*35*). Low molecular mass markers (Sigma, St. Louis, MO) were run parallel to the samples.

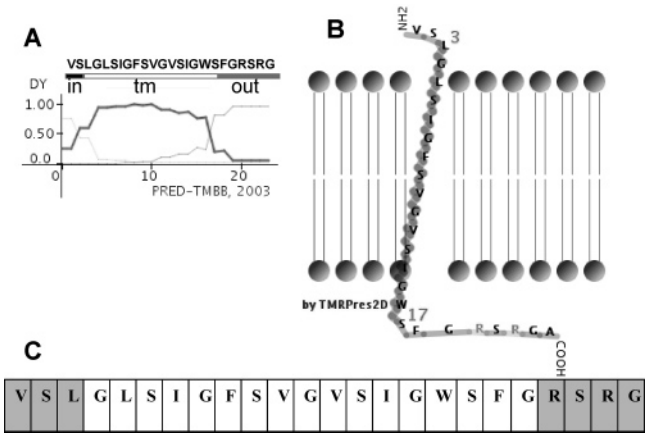

FIGURE 1: Prediction of transmembrane β strands. Output of the prediction obtained from PRED-TMBB for $(xSxG)_6$ peptide (A and B). Plot of the posterior probabilities for transmembrane strands along the given sequence (A) and graphical representation of the predicted topology with respect to lipid bilayer (B). The peptide sequence produced a score of 2.574, which is lower than the threshold value of 2.965, indicating a similarity to outer membrane β barrel proteins. The transmembrane region of the peptide predicted using TM-BETA (C, residues 4−20). The probability of residues to have a β conformation is 0.9−1.0 (residues 5−20), 0.4−0.5 (residue 4), and 0.1−0.2 (residues 1−3).

RESULTS

Prediction of Transmembrane β Strands. Using the PRED-TMBB program the $(xSxG)_6$ sequence produced a score of 2.574, which is lower than the threshold value of 2.965, indicating the possibility of the peptide being related to outer membrane β barrel proteins (*24*). A plot of the posterior probabilities for the transmembrane strands along the sequence and a graphical representation of the predicted topology with respect to the lipid bilayer of the peptide are shown in Figure 1A,B. Utilization of two other publicly available predictors, TM-BETA (http://psfs.cbrc.jp/tmbeta-net/) and B2TMPRED (http://gpcr.biocomp.unibo.it/cgi/predictors/outer/pred_outercgi.cgi), also showed that the amino acid sequence of the peptide is similar to that of outer membrane proteins with a β barrel topology (*25*, *26*). TM-BETA predicts high probability (0.9−1) of a β sheet conformation for residues 5−20 (Figure 1C). B2TMPRED predicts two transmembrane regions (residues 1−11 and 13−20) in the sequence. Taken together, all three methods suggest a β sheet structure in membranes and a possible sequence similarity to outer membrane β barrel proteins.

Conformational Studies. The Fourier deconvoluted ATR-IR spectrum of $(xSxG)_6$ in DMPC/D_2O vesicles is shown in Figure 2. Deuterium oxide (D_2O) was selected as the solvent to avoid interference from arginine side chain absorption in the amide 1 region (*36*). The arginine absorptions near 1635 and 1673 cm^{-1} usually exhibit large shifts of −50 and −70 cm^{-1}, respectively, upon H/D exchange. This was confirmed by a comparative analysis of the secondary derivative spectra in water and D_2O solutions (data not shown). The main feature of the amide 1 region of the spectrum in the D_2O preparation was the occurrence of a strong band around 1627 cm^{-1} and another in the high-frequency region around 1690 cm^{-1}. The spectral bands could be resolved into at least five individual absorptions that are centered around 1694, 1687, 1669, 1652, and 1627 cm^{-1} through deconvolution. The occurrence of a 1627 cm^{-1} band with a high percent relative area (>50%; see Figure 2) revealed a β sheet conformation in membranes (*37*). The high-frequency band found in antiparallel β sheet peptides due to transition dipole coupling is usually very weak compared to the low-frequency band. So, one of the weaker components (1694 cm^{-1}) in the high-frequency region (1660−1700 cm^{-1}) could be ascribed to the antiparallel hydrogen bonding and the rest to turn structures (*38*). A broad band around 1530 cm^{-1} in the amide 2 region (peptide−liposome samples in H_2O) further supported a β sheet structure (data not shown).

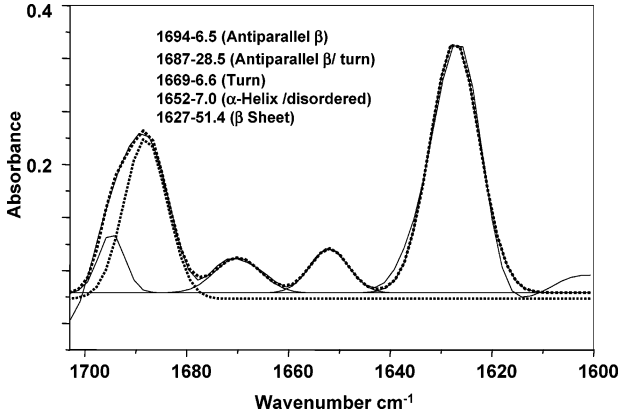

FIGURE 2: ATR-IR spectrum of $(xSxG)_6$ peptide−lipid vesicles in D_2O. Fourier deconvoluted amide 1 bands fitted with a Gaussian function showing five component peaks. The percentage peak area of each component peak and structural assignment corresponding to the peak positions are shown in the inset. On the basis of the peak area of the 1627 cm^{-1} band relative to total area, a lower limit for β sheet content of ~51% could be deduced. Deconvoluted spectra peak width was 12 cm^{-1} and 45% smoothing was used for Gaussian band fitting. The possible errors are ±5% for the peak areas.

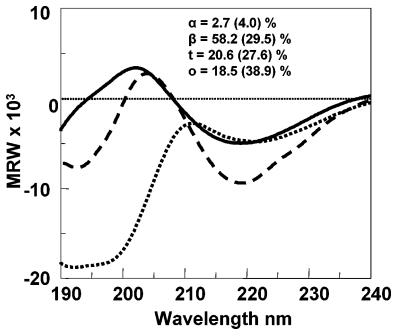

FIGURE 3: CD spectra of $(xSxG)_6$ in membrane mimicking environment and solution. Solid, dashed, and dotted lines represent liposome (peptide/lipid = 1:36) sample and peptide solutions in methanol (0.1 mg/mL) and 75% aqueous methanol, respectively. Secondary structure analysis was performed using the CONTIN/LL method (CDPro software). α, β, t, and o represent fractions of α-helix, β-strand, turn, and unordered components, respectively, of the liposome sample. Values in parentheses indicate corresponding fractions in 100% methanol solution.

The circular dichroism spectra of $(xSxG)_6$ in methanol, 75% aqueous methanol, and liposome solutions were examined to monitor the conformational changes in different environments (Figure 3). The spectrum in methanol showed two negative bands, one near 220 nm and another below 200 nm along with a positive band around 205 nm. In aqueous methanol solution the intensity of the band below 200 nm was increased with a concomitant decrease in the intensity of the 220 nm band. The spectrum of peptide-incorporated liposomes showed a negative band around 220

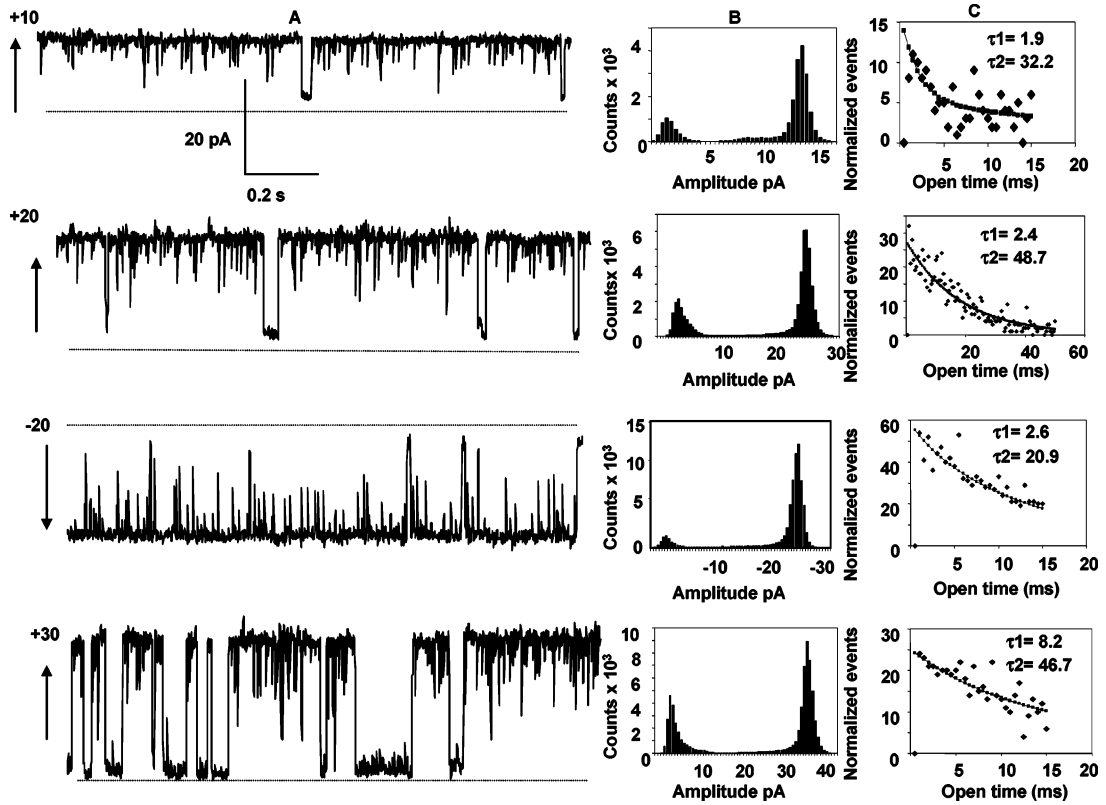

FIGURE 4: Ion channels formed by $(xSxG)_6$ peptide (3 μL of 0.05 mg/mL methanolic solution added to the cis side) at different applied potentials in 1 M CsCl (unbuffered) solution under symmetrical conditions. (A) Channel traces showing high-conductance opening and multi-short-lived closers to subconductance states. Channels open in the direction of arrows, and dotted lines represent zero current level. (B) All-point histograms generated from the corresponding traces on the left showing two levels with a higher probability of channel being in a high-conductance state. (C) The open time distributions generated for the high-conductance state using dwell-time histograms of the data. The binned data (bin width = 0.5 ms) were fitted exponentially using the Marquardt least-squares algorithm. The openings to the large conductance are best characterized with two time constants (τ_1 and τ_2).

nm and a positive band around 202 nm (a negative band below 200 nm was absent). A strong negative band below 200 nm is considered to be a characteristic feature of disordered structures (*39*). A single minimum around 220 nm and a maximum around 200 nm are salient features of the CD spectra of β sheet-rich proteins (*39*). An increase in the intensity of a negative band below 200 nm in aqueous methanol solution could be regarded as a structural change to a more disordered state upon the addition of water to a methanol solution of the peptide. From the CD data, it is presumed that the β sheet content increases in a membrane environment compared to that in solution (*39*). To estimate the approximate fractions of various secondary structures from the CD data, CDPro software package developed by Woody and Sreerama was used (*28*−*31*). The analysis of the CD spectra using the CONTINN/LL method indicated a large fraction of β strand (∼60%; see Figure 3) in the membrane environment compared to that in solution (∼30%). An extended protein basis set of 43 soluble and 13 membrane proteins (basis set 10) was used for analysis. This method utilizes a database containing mainly water-soluble proteins, and hence a quantitative analysis of secondary structural components from CD spectra in a hydrophobic membrane environment is difficult. Nevertheless, it could be used to estimate the relative percentages of different conformational species. A considerable fraction of β turn components were also found from the analysis (*40*). Also, a calculation of the percentages of β sheet and α-helical structures in the membrane environment by comparison with standard polylysine spectra indicates a large fraction (∼53%) of β strand structure (*32*).

Ion Channel Conductance. The peptide incorporation into the lipid bilayer took place immediately after the addition of about 3 μL of a methanolic solution of $(xSxG)_6$ (0.05 mg/mL) to the cis side of the membrane containing 1000 μL of 100−1000 mM electrolyte (final concentration of peptide $\sim 10^{-8}$ M), as evidenced by an increase in membrane conductance and induction of square current events indicating the formation of ion channels. High-conductance channels formed under symmetrical conditions (1 M CsCl, unbuffered) at low applied potentials (10−30 mV) are shown in Figure 4A. At the low applied potentials, the ion channels were in the high-conductance open state most of the time, and complete closures were rarely seen. An important characteristic of the channel was the presence of fast flickering-type events along with several short-lived subconductance states. In many cases, the fast flickering events were the only manifestation of the presence of ion channels due to the complete opening of the channel to a high-conductance state for several minutes. The histograms generated from the channel traces exhibited two broad peaks representative of mainly two conductance states, a closed or low-conductance state and a high-conductance open state (Figure 4B). The proportion of the high-conductance component (the fractional contribution of that component to the area under the curve) obtained by Gaussian fitting of the all-point histogram was found to be always >80% at low membrane potentials. In most patches a mean single channel conductance of 1.37 nS

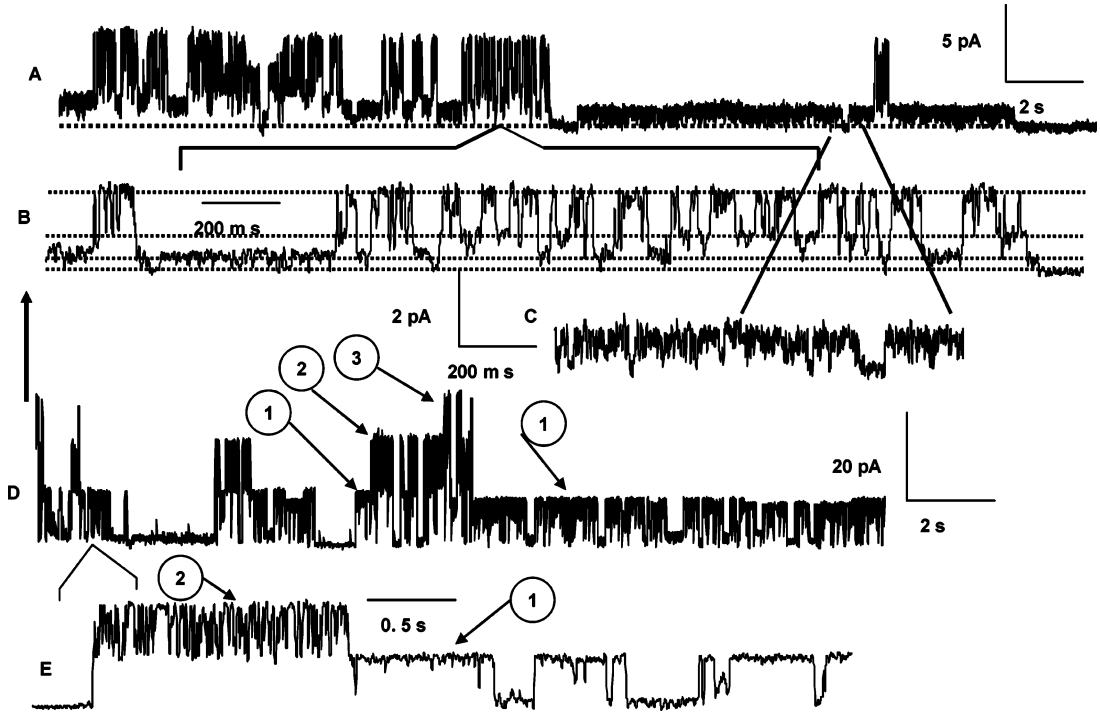

FIGURE 5: Formation of low-conductance channels prior to the induction of high-conductance (1.37 nS) single channels by $(xSxG)_6$. In some experiments low-conductance channels (100 and 500 pS) were seen after the addition of peptide to one side of the bilayer (trace A, conditions same as in Figure 4, applied potential = 10 mV). The two types of channel events are shown in an expanded time scale (B and C). The above channel events were followed by the formation and stabilization of high-conductance channels in the nanosiemens range (1.37 nS) in 2−3 min (D). A part of the channel trace D is shown in an expanded scale (E). Numbers 1, 2, and 3 denote three high-conductance single channels with the same conductance.

was observed. In channel traces, an increase in the number of well-defined subconductance states could be seen with increase in applied potential. This reflects the tendency of the channel to close or return to a low-conductance state at higher membrane potentials as demonstrated earlier (*23*). The ion channel data were further analyzed by generating open time distributions corresponding to the high-conductance state using dwell-time histograms. The binned data were fitted exponentially using the Marquardt least-squares algorithm. The openings to the large-conductance state are best characterized with two time constants (τ_1 and τ_2) at various potentials (Figure 4C).

As mentioned earlier, in most experiments high-conductance channels were immediately (<1−2 min) formed after the addition of $(xSxG)_6$ on one side of the bilayer at low applied potentials. However, in some of the experiments low-conductance channels appeared immediately following the addition of peptide under similar conditions. In Figure 5, the formation of low-conductance channels (100 and 500 pS) after the addition of peptide at an applied potential of 10 mV in 1 M CsCl is shown (trace A). The two types of channel events are shown also in an expanded time scale (traces B and C). These channel events were followed by the formation of high-conductance channels in the nanosiemens range (1.37 nS) in 2−3 min (traces D and E). Three different high-conductance levels shown in the channel trace (numbered 1, 2, and 3) are a simple integer multiple of a single channel conductance (1Λ, 2Λ, and 3Λ, where Λ = 1.37 nS). This suggests that the high-conductance levels (1Λ, 2Λ, and 3Λ) represent the formation of three single channels in this case.

We also examined the effect of peptide concentration on channel activity. However, no correlation between the concentration of peptide added to the bilayer chamber and channel conductance could be obtained. Three stock solutions of the peptide in methanol with concentrations of 100, 50, and 0.1 μg/mL were used and incorporated into the bilayer as explained before (1 M CsCl; applied potential = 10 mV). Surprisingly, even a dilute solution of the peptide (0.1 μg/mL) produced high-conductance channels very similar to that obtained for a 1000 times concentrated sample (100 μg/mL). Ion channels formed after the addition of peptide solution of three different concentrations are shown in Figure 6, demonstrating the formation of a similar type of channels with a mean single channel conductance of 1.37 nS. In some traces spontaneous transition between different well-defined subconductance states could be clearly seen (trace C).

We have observed earlier that the $(xSxG)_6$ channel transports a variety of ions such as Cs^+, K^+, Na^+, Li^+, Ca^{2+}, NH_4^+, NMe_4^+, NEt_4^+, NEt_3Bz^+, Cl^-, and glucosammonium and has little preference to cations over anions (*23*). Assuming the pore to be a perfect water-filled cylinder of about 6 nm in length and filled with an aqueous solution having a specific conductance (σ) of about 110 mS/cm (1 M KCl), a pore diameter of about 10.2 Å could be deduced from the mean single channel conductance (Λ) of 1.5 nS using the equation $\Lambda = \sigma\pi r^2/l$, where r is the radius and l is the length of the pore (*13*). This value could be considered as a lower limit of the pore diameter as it is derived on the assumption of negligible interaction between pore interior and moving ions and is consistent with the movement of large cations such as NEt_3Bz^+ (10. 5 Å, conductance = 80 pS in 100 mM solution under symmetrical conditions) and

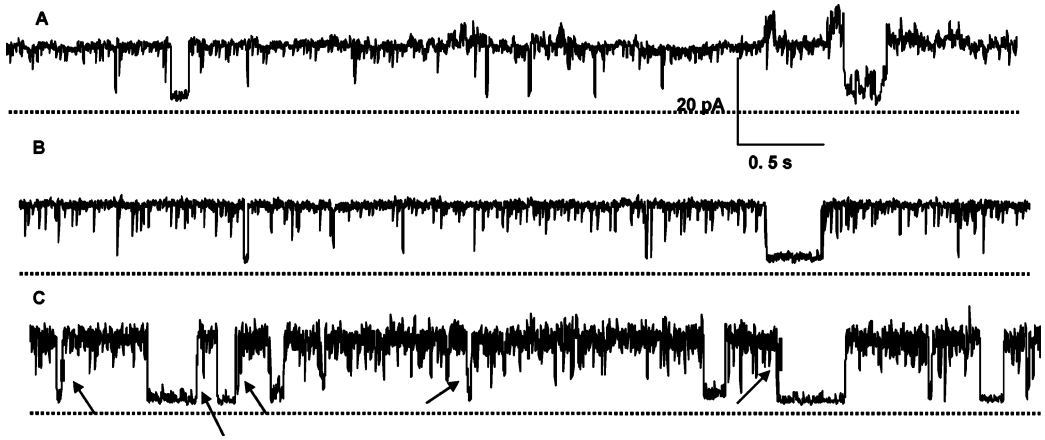

FIGURE 6: Effect of peptide concentration on channel conductance. Ion channels formed after the addition of 3 μL of methanolic solutions of $(xSxG)_6$ having three different concentrations (trace A, 0.1 μg/mL; trace B, 50 μg/mL; trace C, 100 μg/mL), demonstrating the formation of a similar type of channels with a mean single channel conductance of 1.37 nS (applied potential, 10 mV; 1 M CsCl; experimental conditions same as in Figure 4). Spontaneous transitions between different subconductance levels are indicated by arrows.

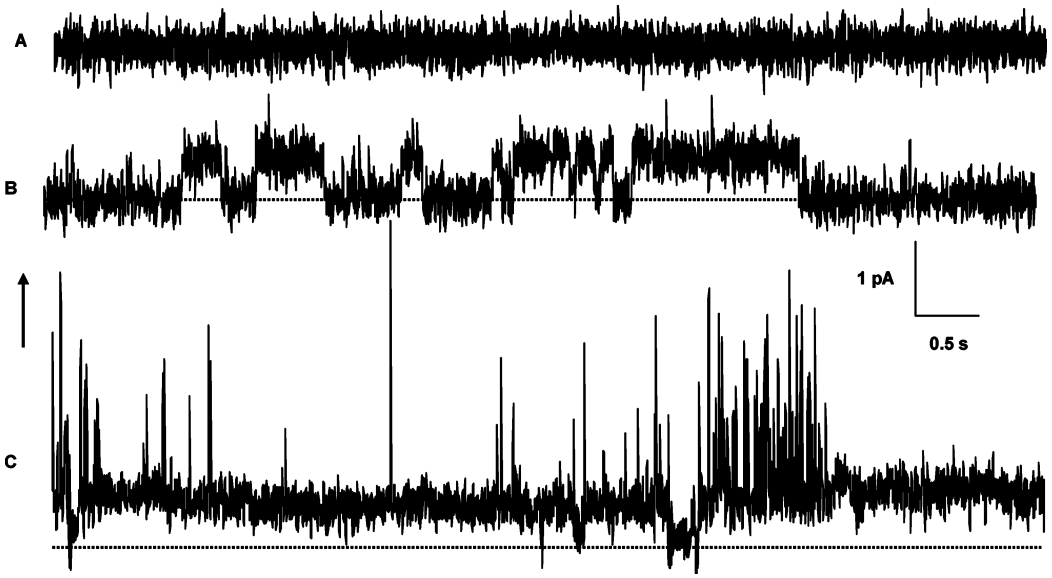

FIGURE 7: Inhibition of $(xSxG)_6$ ion channels by Congo red. Ion channels were not observed upon the coaddition of the peptide and Congo red (0.05 mg/mL methanolic solution of the peptide mixed with 12 μM Congo red solution) to the bilayer chamber under voltage clamp conditions (trace A; applied potential, 10 mV; 1 M CsCl). Formation of low-conductance channels (trace B) and induction of high-conductance channels (trace C) after the removal of Congo red containing solution and subsequent addition of peptide solution (0.05 mg/mL methanolic solution) without Congo red.

glucosammonium (10 Å, conductance = 130 pS in 100 mM solution) through the pore.

Congo red is known to bind active peptide aggregates, thereby inhibiting channel formation (*7*). To determine whether the ion channels were formed through peptide aggregation, the effect of Congo red on channel formation was examined by adding a peptide solution containing Congo red (0.05 mg/mL methanolic solution of the peptide mixed with 12 μM Congo red solution) to the bilayer chamber under voltage clamp conditions (10 mV, 1 M CsCl). Ion channels were not observed under these conditions, indicating the inhibition of channel formation by Congo red (Figure 7A). Removing the bilayer solution containing Congo red and subsequent addition of peptide solution without Congo red during the experiment resulted in the induction of low-conductance channels followed by fluctuation showing the formation of high-conductance channels (Figure 7B,C). These results suggest that peptide aggregates in the aqueous phase are responsible for channel formation.

Electron Microscopy. Electron microscopy (EM) was used to investigate $(xSxG)_6$ aggregation in aqueous and membrane environments. The electron micrographs of negatively stained peptide samples under different conditions are shown in Figure 8. A freshly prepared suspension of the peptide in water (0.2 mg/mL) formed small amorphous-like aggregates, which do not have a well-defined structure (Figure 8A). Incubation of the sample at 60 °C for 2−3 h resulted in the formation of well-defined short fibril structures with an average diameter of about 8 nm (Figure 8B) and after extensive aging (2 months) long fibrillar structures resembling amyloid fibrils were formed (Figure 8C). The electron micrographs of liposome samples revealed the formation of almost uniformly sized unilamellar vesicles (average diameter of ~100 nm; Figure 8D−I). The formation of oligomeric species after the addition of a methanolic solution of (0.01 mg/mL) peptide to preformed liposomes is shown in Figure 8D−G. In fresh liposome−peptide samples short fibrillar structures were seen primarily concentrated near liposomes

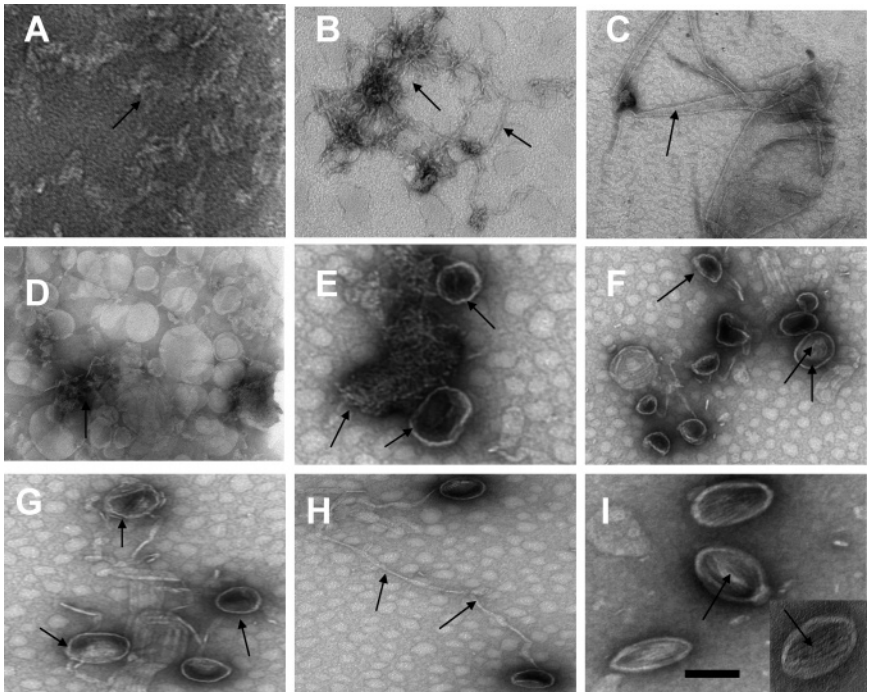

FIGURE 8: Electron micrographs of $(xSxG)_6$ peptide fibrils and interaction of oligomers with liposomes. (A) Peptide aggregates formed in a freshly prepared suspension in water (0.2 mg/mL). (B) Formation of short fibrils after incubation in water at 60 °C. (C) Long fibrils appeared after aging sample B for several days. (D, E) Formation of oligomeric species after the addition of a methanolic solution of (0.01 mg/mL) peptide to preformed liposomes; oligomeric species localized around the vesicles are clearly visible in fresh liposome−peptide samples. (F, G) In vortexed liposome−peptide samples (vortexed for 5 min followed by incubation for 2 h before EM experiments) the vesicles decorated with the peptide and oligomers that are primarily concentrated on the edges of the bilayer can be seen. (H) Incubation of the peptide−liposome sample G at 40 °C for about 1 h led to the formation of large fibrils similar to that observed in aged peptide samples in water. (I) EM of a peptide incorporated liposome sample made by sonication (see Materials and Methods section) showing lesions inside the bilayer possibly representing peptide oligomers. Arrows represent peptide oligomeric species, and the bar corresponds to 50 nm.

than in the bulk (Figure 8D,E). Also, oligomeric species localized around the vesicles were clearly visible in these samples (Figure 8E). In vortexed liposome−peptide samples (vortexed for 5 min followed by incubation for 2 h before EM experiments) the vesicles were decorated with the peptide, and oligomers could be detected primarily on the edges of the bilayer (Figure 8F,G). Incubation of the peptide−liposome sample at 40 °C for about 1 h led to the formation of large fibrils similar to that observed in aged peptide samples in water (Figure 8H). We also examined the electron micrographs of peptide-incorporated liposome samples made by sonication (see Materials and Methods section) and noticed that the oligomeric species were not prevalent outside liposomes; however, lesions indicating the oligomeric species inserted into the bilayer were observed (Figure 8I).

Congo Red Binding. Congo red is a useful dye to detect the formation of amyloid fibrils. It has been shown to bind preferentially to aggregated peptides/proteins of amyloid but not to the native, unassembled forms (*7*, *34*). We performed the Congo red binding experiments to examine whether the aggregates of $(xSxG)_6$ have the characteristics of the amyloid fibril. The ultraviolet absorbance spectra of Congo red in the absence and presence of a suspension of peptide fibrils are shown in Figure 9. Significant red shift (∼23 nm) was observed in the absorption spectrum when the dye was bound to the peptide in the aggregated state and is in accordance with the electron microscopy results. Such a prominent red shift in the absorption maxima is attributed to the strong

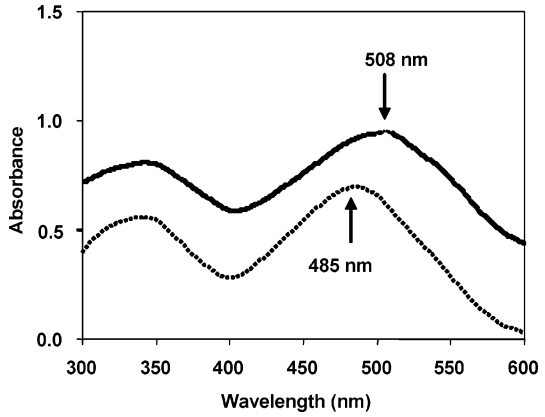

FIGURE 9: Congo red binding to β sheet aggregates. The ultraviolet absorbance spectra of Congo red in the absence (dotted line) and presence of a suspension of $(xSxG)_6$ fibrils (solid line) in 0.1 M NaCl. A significant red shift (∼23 nm) is observed when the dye binds to peptide aggregates.

intercalation of the dye into the ordered intermolecular β pleated sheet structure of the peptide fibrils (*7*).

Gel Electrophoresis. When the $(xSxG)_6$-incorporated liposomes were electrophoresed on a Tricine−SDS−polyacrylamide gel, at least four bands with molecular masses close to ∼6, 20, 29, and 45 kDa representing dimeric and multimeric peptide species were detected (Figure 10, lane c). A freshly prepared solution of the peptide in DMSO showed a single band apparently indicating the presence of monomeric peptide species (lane d). Lanes a and b represent standard molecular mass markers and a liposome sample

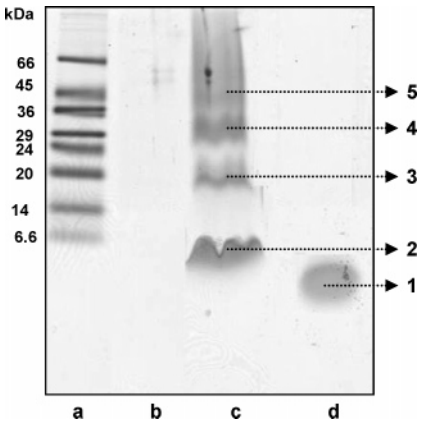

FIGURE 10: Tricine−SDS−polyacrylamide gel electrophoresis of $(xSxG)_6$ incorporated liposomes showing at least four bands with molecular masses close to ~6, 20, 29, and 45 kDa representing dimeric and multimeric peptide species (lane c). A freshly prepared solution of the peptide in DMSO exhibits a single band apparently indicating the presence of monomeric species (lane d). Lanes a and b represent standard molecular mass markers and a liposome sample (DMPC) without the peptide, respectively. The samples were run in 16.5% polyacrylamide gels, followed by staining with Coomassie Blue.

without the peptide, respectively. These results indicate that $(xSxG)_6$ forms stable oligomeric structures in the lipid bilayer membranes.

DISCUSSION

In general, the electrophysiological characteristics of β barrel porins can be summarized as follows: (i) there is formation of highly conductive ion channels (in nanosiemens range), (ii) the channels with large conductances are maximally open at low potentials around 0 mV and close at higher positive and negative potentials >100 mV, (iii) the channels exhibit both fast and slow kinetics on very different time scales, and (iv) the channels exhibit several subconducting states (*19*−*21*). The ion channel properties of $(xSxG)_6$ are found to be similar to that of porins in several respects. The formation of highly conductive nonselective channels, the two-state gating of the channels at potentials $>\pm 40$ mV, the observation of fast and slow kinetic events, and the existence of subconductance states demonstrate such a similarity (*23*). On the basis of these results it is reasonable to believe that such a similarity could be due to the formation of a structure close to that of β barrel porin channels. This is further supported by CD and IR studies indicating a β sheet conformation in membranes stabilized by antiparallel hydrogen bonding and possibly some β turns. The permeation of a wide variety of ions of different sizes suggests the formation of nonselective channels with a pore diameter >10.5 Å. Low cation selectivity in the presence of a KCl concentration gradient indicates only a minor interaction of ions with the pore interior despite the presence of six serine hydroxyls which would be possibly arrayed in the same direction in a β sheet structure (*23*). Also, it seems that the presence of two positively charged arginine residues does not influence the ion selectivity. This could be related to the larger size of the pore. The pore diameter calculated from single channel conductance is only approximate due to the assumption of a cylindrical pore and free moving ions without any interaction with the pore interior. Nevertheless, the calculated pore diameter (~11 Å) is close to that reported for several porins (*13*, *41*).

Formation of porin-like ion channels by a short peptide would naturally prompt one to ask questions such as why does this peptide show conformational and electrophysiological similarities to that of β barrel porins? Is there any sequence similarity between this peptide and porins? Having noticed the β structure of this peptide in lipid membranes, the first attempt toward an answer would be to check for any sequence homology to common β barrel proteins. Using different web-based programs, PRED-TMBB, TM-BETA, and B2TMPRED, we observed an apparent sequence similarity to that of β barrel outer membrane proteins of Gram-negative bacteria as described in the Results section (*24*−*26*). Membrane-spanning β strands, like all β sheets, have a dyad repeat topology in which alternating residues are oriented toward alternating faces of the sheet. In β barrel membrane proteins about half of the membrane-spanning residues are hydrophobic residues while the other half are more hydrophilic residues that are oriented toward the interior of the barrel (*42*). Leucine and valine are the most abundant external β barrel residues. Aromatic residues phenylalanine and tryptophan are also abundant on the external surface. Glycine and serine are the most abundant internal residues (*42*). In the sequence VSLGLSIGFSVGVSIGWSFGRSRG a β sheet structure would place more hydrophilic serine and glycine residues on one side and hydrophobic residues on the opposite side. Hence, a dyad repeat sequence combined with the presence of glycine, serine, and hydrophobic residues in a repeated pattern in the case of the present peptide may provide a favorable condition for the formation of β barrels in membranes.

It has been proposed that short-lived substates found in the ion channel traces of porins represent the flickering of monomer channels between open and closed states whereas large-conductance openings represent multimer channels (*21*). In the present case the kinetic analysis of open channels showed that the large-conductance opening events could not be modeled by a single time constant, suggesting that the high-conductance opening events represent a complex channel. Usually, such channels could result from the cooperation of several individual pore-forming protein units, or an individual pore-forming unit could adopt distinct conformations resulting in multiple conductance states (*43*). If direct transitions between two or more conductance levels occur (interconverting conductances), such levels could be considered as subconductance states of the same channel (*5*, *14*). In some experiments interconversion among different conductance levels could be clearly resolved. Figure 11 demonstrates transition between different conductance states in both picosiemen and nanosiemen range. In trace A, transition between current levels with conductance 110−590, 110−1000, 110−1300, 590−1000, 590−1300 pS, etc. can be clearly identified. Trace B also shows transition between different well-defined conductance levels such as 110−335 and 235−550 pS and vice versa. Trace C demonstrates multiple interconverting transitions between several low-conductance levels. Examples of direct transition between two or more conductance levels are also shown in Figure 6. The existence of interconverting transitions between different conductance levels indicates that those levels are subconductance states of the same channel. An interesting type of

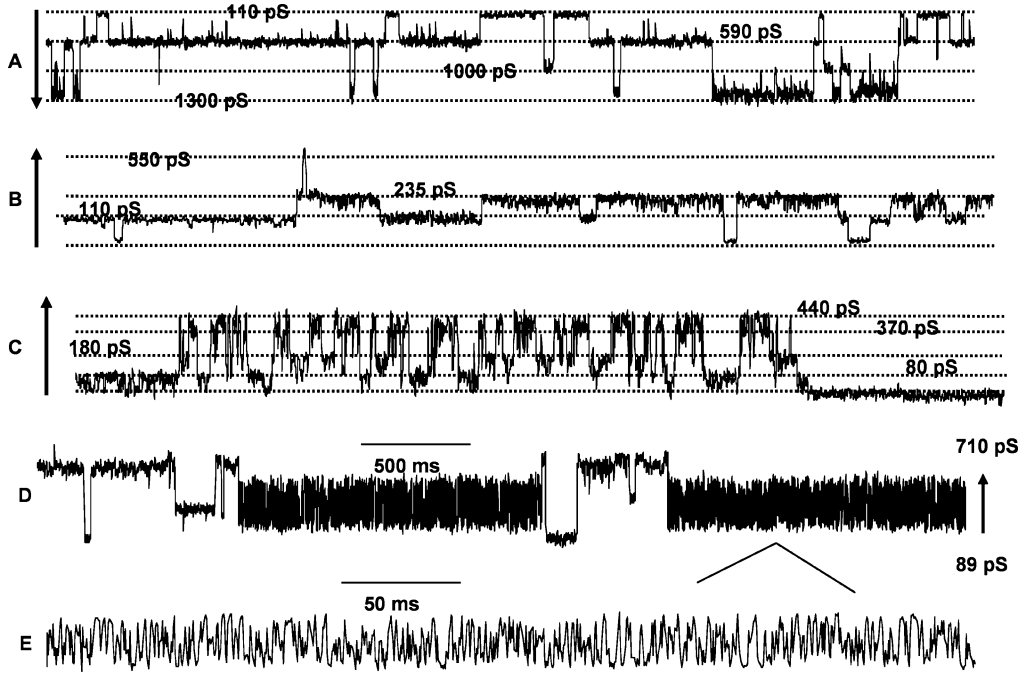

FIGURE 11: Interconverting multiple transitions observed in $(xSxG)_6$ channels. Transitions between different conductance states in both picosiemen and nanosiemen range are shown. (A) Transitions between conductance levels 110−590, 110−1000, 110−1300, 590−1000, and 590−1300 pS. (B) Transitions between different well-defined conductance levels, 110−335 and 235−550 pS and vice versa. (C) Demonstration of multiple interconverting transitions between several low-conductance levels. (D, E) High-frequency transitions along with low-frequency transitions (experimental conditions are the same as in Figure 4; applied potential, 10 mV; 1 M CsCl).

high-frequency transitions also occurred along with low-frequency transitions just like that reported for Aβ (1−40) and porin channels (Figure 11C,D) and is regarded as an indication of hindrance of ion flow through the open pore (*5*).

Formation of porin-like channels suggests self-assembly of $(xSxG)_6$ into multimers and as possible structural species responsible for its ion channel activity. It is reasonable to believe that a short peptide that has only 24 amino acids is of insufficient length to fold into a β barrel structure similar to outer membrane porins. In this respect, the membrane insertion and folding of these peptides are more likely to be similar to that of pore-forming toxin channels. It is known that large β barrel pores found in pore-forming toxins have an oligomeric structure formed by the association of inactive monomers. For example, in α-hemolysin pores, each monomer subunit contributes two β strands and forms a heptameric 14-stranded antiparallel β barrel (*44*). Compared to outer membrane porins, the PFT channels switch to a closed state at a lower membrane potential of ∼50 mV (*17*, *18*). The $(xSxG)_6$ channels also tend to close around 50 mV, suggesting a similarity to oligomeric PFT channels (*23*). In several β sheet peptides such as β amyloids the ion channels are thought to be formed by peptide oligomerization, though the exact nature of such structures is not known (*7*). On the basis of the ion channel characteristics of amyloid β peptides, it was postulated that the structure of small β sheet and aggregating peptides may be uniquely suitable to channel formation, perhaps by forming β barrels similar to that of porins (*7*). Amyloid β peptides also form high-conductance multimeric channels in membranes; however, a voltage-gating behavior similar to porins has not been detected.

The evidence that the peptide aggregate is needed for channel formation was obtained from Congo red binding studies. The inhibition of channel formation by Congo red must be due to the loss of active aggregates as it inserts into β pleated sheet structure, thereby preventing aggregation (*7*). This strongly suggests that only peptide aggregates but not monomers form channels. A general mechanism of β barrel pore formation by PFTs involves the formation of a membrane-bound prepore oligomer from a membrane-bound monomer and insertion of the oligomer into the membrane followed by pore formation via cooperative events (*45*). Due to the hydrophobic nature and poor solubility of $(xSxG)_6$ in water unlike β-PFTs, we believe that the addition of a methanolic solution of the peptide to a high ionic strength salt solution during bilayer experiments would lead to the spontaneous aggregation of the peptide into a oligomeric structure before it is finally inserted into the membrane and possibly folded into a β barrel-like structure. Moreover, in this study the channel conductance was found to be similar over a wide range of peptide concentrations (Figure 6), suggesting that same type of peptide aggregates is formed irrespective of the amount of peptide added to the bilayer chamber and inserted into the membrane. Oligomerization of the peptide into fibrillar structures in an aqueous environment is revealed by electron microscopy. Furthermore, the observation of oligomeric structures in association with lipid vesicles suggests insertion of the peptide as polymeric species into lipid bilayers. Liposomes decorated with peptide oligomeric species were seen during peptide−liposome binding studies as well as in the case of sonicated peptide−lipid vesicles. In an aqueous environment the formation of short fibrillar structures occurs under harsh conditions (incubation at 60 °C for 2−3 h), whereas in the presence of lipid bilayers it seems that the aggregation into fibrillar structures is facilitated even under milder conditions (immediately after the addition of a methanolic solution of peptide to preformed

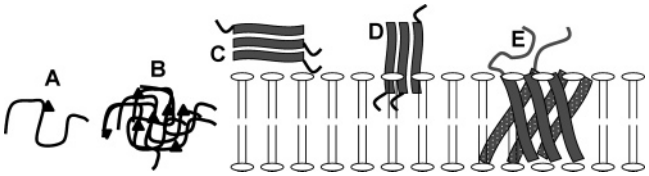

FIGURE 12: Schematic representation of the possible pathway of channel formation by $(xSxG)_6$ peptide. (A, B) The addition of a dilute methanolic solution (3 μL of 100−0.1 μg/mL) of the peptide (partially folded and possibly monomeric) to the bilayer chamber containing high ionic strength salt solution (1 M) would lead to the spontaneous aggregation into a more disordered state. (C) The peptide aggregate interacts with the membrane surface, resulting in a conformational change to a β sheet-rich structure followed by aggregation into well-ordered oligomeric species. (D, E) The oligomer inserts into the bilayer and folds into a β barrel-like structure inside the hydrophobic membrane.

liposomes at room temperature). CD studies have shown that $(xSxG)_6$ is only partially folded in methanol, as indicated by the large fraction of unordered and β turn components from secondary structure analysis. Upon binding to lipid bilayers the peptide adopts a conformation rich in β sheet secondary structure compared to that in solution. These observations are consistent with the finding of a lipid-induced β sheet aggregation in Aβ peptides (*8*, *9*). A plausible pathway for a β barrel-like channel formation could be proposed on the basis of the above discussion (Figure 12). The addition of a dilute methanolic solution (100−0.05 μg/mL) of $(xSxG)_6$ (partially folded) to the bilayer chamber containing high ionic strength salt solution (1 M) would lead to the spontaneous aggregation of the peptide into a more disordered state (as shown by CD in aqueous methanol). The peptide aggregate then interacts with the membrane surface, resulting in a conformational change to a β sheet-rich structure followed by aggregation into well-ordered oligomeric species. In the next step the oligomer inserts into the membrane and folds into a β barrel-like structure inside the hydrophobic interior (Figure 12). The energetic barrier for inserting into the membrane could be circumvented if the β strands are inserted as multimeric β sheets and form closed structures such as a β barrel (*17*).

The formation of low-conductance channels in some experiments prior to the appearance of large-conductance channels may be due to the presence of smaller peptide aggregates which can further self-assemble to form larger pores. Hence it is presumed that the size of the pore and channel conductance depend on the extent of peptide aggregation and number of peptide subunits. In this type of structure, each peptide subunit (smaller aggregates) also could behave as an ion channel. In this way such channels would resemble complex porin channels which are themselves multimers of more than one β barrel pore. The electrophoresis of $(xSxG)_6$-incorporated liposomes revealed the existence of at least three stable multimeric structures along with dimeric species. This indicates that the ion channel may be composed of a different number of subunits. We propose that short-lived subconductance states associated with high-conductance single channels represent transitions between open and closed states of individual peptide subunits. A large peptide pore formed by the association of several individual β sheets or smaller β sheet aggregates is thus expected to have a complex behavior in membranes. Also, a dynamic assembly−disassembly process is possible inside the membrane where a peptide oligomeric pore is in equilibrium with individual peptide units of different sizes.

The $(xSxG)_6$ peptide has an amphipathic β structure in membranes and shows a functional similarity to β barrel proteins. We believe that due to these characteristics such synthetic peptides would provide useful model systems for establishing the fundamental thermodynamic and structural principles of folding in β barrel proteins and to understand the mechanism of two-state voltage gating (*46*). Moreover, β sheet peptides having a dyad repeat sequence, and appropriately placed glycine, serine, and hydrophobic residues may be suitable for mimicking pore characteristics of β barrel proteins. The unprecedented observation of both a porin-like ion channel activity and formation of oligomeric species by a short synthetic β-sheet peptide indicates self-assembly into a β barrel-like structure as one of the possible mechanisms for channel formation by β sheet peptides. We also expect a structural role for glycine in porin-like ion channel formation and aggregation. In future studies the effect of glycine in these peptides will be worthy of closer examination, as glycine is one of the most abundant amino acids in the membrane-spanning β strands of naturally occurring β barrel membrane proteins (*42*). Moreover, several amyloid β peptides have an appreciable fraction of glycine residues, in some cases in a repeating pattern (*47*).

ACKNOWLEDGMENT

The authors thank Cary Pritchard, Department of Chemistry, IUPUI, Indianapolis, IN, for technical assistance with CD and ATR-IR spectroscopic analysis, Caroline A. Miller, Electron Microscopy Center, IUPUI, for electron micrographs of peptides, and Zhidong Zhang for helping in the mass spectroscopic analysis.

REFERENCES

1. Trzesniewska, K., Brzyska, M., and Elbaum, D. (2004) Neurodegenerative aspects of protein aggregation, *Acta Neurobiol. Exp. 64*, 41−52.
2. Selkoe, D. J. (2003) Folding of proteins in fatal ways, *Nature 426*, 900−904.
3. Rochet, J.-C., and Landsbury, P. T. (2000) Amyloid fibrillogenesis: themes and variations, *Curr. Opin. Struct. Biol. 10*, 60−68.
4. Kelly, J. W. (1996) Alternative conformations of amyloidogenic proteins govern their behavior, *Curr. Opin. Struct. Biol. 6*, 11−17.
5. Arispe, N., Pollard, H. B., and Rojas, E. (1993) Giant multilevel cation channels formed by Alzheimer disease amyloid beta protein [AβP-(1−40)] in bilayer membranes, *Proc. Natl. Acad. Sci. U.S.A. 90*, 10573−10577.
6. Arispe, N. (2004) Architecture of the Alzheimers AβP ion channel pore, *J. Membr. Biol. 197*, 33−48.
7. Hirakura, Y., Lin, M.-C., and Kagan, B. L. (1999) Alzheimers amyloid Aβ 1−42 channels: Effects of solvent, pH and Congo red, *J. Neurosci. Res. 57*, 458−466.
8. Terzi, E., Holzeman, G., and Seelig, J. (1995) Self-association of β-amyloid peptide (1−40) in solution and binding to lipid membranes, *J. Mol. Biol. 252*, 633−642.
9. Kazlauskaite, J., Sanghera, N., Sylvester, I., Bryan, C. V., and Pinheiro, T. J. T. (2003) Structural changes of the prion protein in lipid membranes leading to aggregation and fibrillization, *Biochemistry 42*, 3295−3304.
10. Lin, M.-C. A., and Kagan, B. L. (2002) Electrophysiological properties of channels induced by Aβ25−35 in planar lipid bilayers, *Peptides 6414*, 1−14.
11. Krantz, D. D., Zidovetzki, R., Kagan, B. L., and Zipursky, S. L. (1991) Amphipathic β structure of a leucine-rich repeat peptide, *J. Biol. Chem. 266*, 16801−16807.

12. Lin, H., Bhatia, R., and Lal, R. (2001) Amyloid β protein forms ion channels: implications for Alzheimer's disease pathophysiology, *FASEB J. 15*, 2433−2444.
13. Benz, R., Schmid, A., and Hancock, R. W. (1983) Ion selectivity of gram-negative bacterial porins, *J. Bacteriol. 153*, 241−252.
14. Hill, K., Model, K., Ryan, M. T., Dietmeier, K., Martin, F., Wagner, R., and Pfanner, N. (1998) Tom40 forms the hydrophilic channel of the mitochondrial import pore for preproteins, *Nature 395*, 516−521.
15. Schleiff, E., Soll, J., Kuchler, M., Kuhlbrandt, W., and Harrer, R. (2003) Characterization of the translocon of the outer envelope of choloroplasts, *J. Cell Biol. 160*, 541−551.
16. Wimley, W. C. (2003) The versatile β-barrel membrane protein, *Curr. Opin. Struct. Biol. 13*, 404−411.
17. Heuck, A. P., Tweten, R. K., and Johnson, A. E. (2001) β-Barrel pore forming toxins: intriguing dimorphic proteins, *Biochemistry 40*, 9065−9073.
18. Chakraborthy, T., Schmid, A., Notermans, S., and Benz, R. (1990) Aerolysin of *Aeromonas* sorbia: Evidence for formation of ion permeable channels and comparison with alpha-toxin of *Staphylococcus aureus*, *Infect. Immun. 58*, 2127−2132.
19. Conlan, S., Zhang, Y., Cheley, S., and Bayley, H. (2000) Biochemical and biophysical characterization of OmpG: A monomeric porin, *Biochemistry 39*, 11845−11854.
20. Bainbridge, G., Gokce, I., and Lakey, J. H. (1998) Voltage gating is a fundamental feature of porin and toxin β-barrel membrane channels, *FEBS Lett. 431*, 305−308.
21. Berrier, C., Coulombe, A., Houssin, C., and Ghazi, A. (1992) Fast and slow kinetics of porin channels from *Escherichia coli* reconstituted into giant liposomes and studied by patch-clamp, *FEBS Lett. 306*, 251−256.
22. Chaney, M. O., Webster, S. D., Kuo, Y., and Roher, A. E. (1998) Molecular modeling of the Aβ 1−42 peptide from Alzheimer's disease, *Protein Eng. 11*, 761−767.
23. Thundimadathil, J., Roeske, R. W., and Guo, L. (2005) A synthetic peptide forms voltage-gated porin-like ion channels in lipid bilayer membranes, *Biochem. Biophys. Res. Commun. 330*, 585−590.
24. Bagos, P. G., Liakopoulos, T. D., Spyropoulos, I. C., and Hamodrakas, S. J. (2004) PRED-TMBB: a web server for predicting the topology of β barrel outer membrane proteins, *Nucleic Acids Res. 32*, W400−W404.
25. Jacoboni, I., Martelli, P. L., Fariselli, P., De Pinto, V., and Casadio, R. (2001) Prediction of the transmembrane regions of β-barrel membrane proteins with a neural network-based predictor, *Protein Sci. 10*, 779−787.
26. Gromiha, M. M., Ahmad, S., and Suwa, M. (2004) Neural network-based prediction of transmembrane beta-strand segments in outer membrane proteins, *J. Comput. Chem. 25*, 762−767.
27. Wallace, B. A., and Blout, E. R. (1979) Conformation of an oligopeptide in phospholipid vesicles, *Proc. Natl. Acad. Sci. U.S.A. 76*, 1775−1779.
28. Sreerama, N., and Woody, R. W. (1993) A self-consistent method for the analysis of protein secondary structure from circular dichroism, *Anal. Biochem. 209*, 32−44.
29. Johnson W. C., Jr. (1988) Secondary structure of proteins through circular-dichroism spectroscopy, *Annu. Rev. Biophys. Biophys. Chem. 17*, 145−166.
30. Provencher, S. W., and Glockner, J. (1981) Estimation of globular protein secondary structure from circular dichroism, *Biochemistry 20*, 33−37.
31. Sreerama, N., and Woody, R. W. (2004) On the analysis of membrane protein circular dichroism spectra, *Protein Sci. 13*, 100−112.
32. Zhong, L., and Johnson, W. C., Jr. (1992) Environment affects amino acid preference for secondary structure, *Proc. Natl. Acad. Sci. U.S.A. 89*, 4462−4465.
33. Benz, R., Janko, K., Boos, W., and Lauger, P. (1978) Formation of large, ion-permeable membrane channels by the matrix protein (porin) of *Escherichia coli*, *Biochim. Biophys. Acta 511*, 305−319.
34. Lazo, N. D., and Downing, D. T. (1997) β-Helical fibrils from a model peptide, *Biochem. Biophys. Res. Commun. 235*, 675−679.
35. Schagger, H., and von Jagow, G. (1987) Tricine-sodium dodecyl sulfate-polyacrylamide gel electrophoresis for the separation of proteins in the range from 1 to 100 kDa, *Anal. Biochem. 166*, 368−379.
36. Chirgadze, Y. N., Fedorov, O. V., and Trushima, N. P. (1975) Estimation of amino acid residue side chain absorption in the infrared spectra of protein solutions in heavy water, *Biopolymers 14*, 679−694.
37. Barth, A., and Zscherp, C. (2002) What vibrations tell us about proteins, *Q. Rev. Biophys. 35*, 369−430.
38. Jackson, M., and Mantsch, H. H. (1995) The use and misuse of FTIR spectroscopy in the determination of protein structure, *Crit. Rev. Biochem. Mol. Biol. 30*, 95−120.
39. Sreerama, N., and Woody, R. W. (2004) Computation and analysis of protein circular dichroism spectra, *Methods Enzymol. 383*, 318−351.
40. Sreerama, N., and Woody, R. W (2004) On the analysis of membrane protein circular dichroism spectra, *Protein Sci. 13*, 100−112.
41. Palmer, M., Harris, R., Freytag, C., Kehoe, M., Tranum-Jenson, J., and Bhakdi, S. (1998) Assembly mechanism of the oligomeric streptolysin O pore: the early membrane lesion is lined by a free edge of the lipid membrane and is extended gradually during oligomerization, *EMBO J. 17*, 1598−1605.
42. Wimley, W. C. (2002) Toward genomic identification of β-barrel membrane proteins: Composition and architecture of known structures, *Protein Sci. 11*, 301−312.
43. Minn, A. J., Velez, P., Schendel, S. L., Liang, H., Muchmore, S. W., Fesik, S. W., Fill, M., and Thompson, C. B. (1997) Bcl-XL forms an ion channel in synthetic lipid membranes, *Nature 385*, 353−357.
44. Gouaux, J. E., Braha, O., Hobaugh, M. R., Song, L., Cheley, S., Shustak, C., and Bayley, H. (1994) Subunit stoichiometry of staphylococcal α-hemolysin in crystals and on membranes: A heptameric transmembrane pore, *Proc. Natl. Acad. Sci. U.S.A. 91*, 12828−12831.
45. Valeva, A., Weisser, A., Walker, B., Kehoe, M., Bayley, H., Bhakdi, S., and Palmer M. (1996) Molecular architecture of a toxin pore: a 15-residue sequence lines the transmembrane channel of staphylococcal alpha-toxin, *EMBO J. 15*, 1857−1864.
46. Wimley, W. C., Hristova, K., Ladokhin, A. S., Silvestro, L., Axelsen, P. H., and White, S. H. (1998) Folding of β-sheet membrane proteins: A hydrophobic hexapeptide model, *J. Mol. Biol. 277*, 1091−1110.
47. Liu, W., Crocker, E., Zhang, W., Elliott, J. I., Luy, B., Li, H., Aimoto, S., and Smith, S. O. (2005) Structural role of glycine in amyloid fibrils formed from transmembrane α-helices, *Biochemistry 44*, 3591−3597.

BI0508643